Unsupervised change detection using texture difference measure for VHR remote sensing images

ZHENXUAN LI†, WENZHONG SHI*‡, HUA ZHANG† and MING HAO†

† School of Environment Science and Spatial Informatics, China University of Mining and Technology, Xuzhou, China

‡ Joint Research Laboratory on Spatial Information, The Hong Kong Polytechnic University and Wuhan University, Hong Kong and Wuhan, China

In this paper, an unsupervised change detection method is proposed by using texture difference information for very-high-resolution (VHR) remote sensing images. First, a new local similarity based texture difference measure (LSTDM) is defined by using gray level co-occurrence matrix (GLCM). A mathematical analysis shows that LSTDM is robust with respect to noise and spectral similarity. Then, the unsupervised change detection problem in VHR remote sensing images is formulated as minimizing an energy function related with changed and unchanged classes in the difference image. A modified expectation maximization based active contour model is applied to the difference image for separating the changed and unchanged regions. Finally, two different experiments were performed with SPOT5 images and QuickBird images and compared with some state-of-the-art unsupervised change detection methods to evaluate the effectiveness of the proposed method. The results indicate that the proposed method can sufficiently increase the robustness with respect to noise and spectral similarity and obtain the highest accuracy among methods in this paper.

1 Introduction

Change detection is a process that identifies the changes occurred on the Earth surface by jointly observing two (or more) images acquired on the same geographical area at different times (Bruzzone and Prieto 2000; Lu et al. 2004; Bruzzone and Bovolo 2013). Recently, it is more convenient to obtain a series of multi-temporal optical satellite images with the development of remote sensing techniques. Under this background, land cover change detection from remote sensing images has been becoming an attractive research topic.

In the past few decades, a variety of change detection methods have been proposed. According to the existence of ground truth in the interesting area, the change detection approaches can be divided into supervised approach and unsupervised approach. Due to the ground truth is difficult to obtain and cost too much, the unsupervised approach has been more widely researched. In this paper, we focus on the unsupervised change detection methods. In order to separate changed pixels from unchanged pixels in the difference image, the most popular unsupervised change detection method is a thresholding technique (Prieto and Fernandez 2000; Bazi, Bruzzone, and Melgani 2005; He et al. 2014) for its simplicity and availability. Additionally, in order to obtain more accurate change detection result, some literatures proposed automatic analysis and other new techniques for the difference image instead of a thresholding method,

such as support vector machine (Bovolo, Bruzzone, and Marconcini 2008), wavelet transform (Bovolo and Bruzzone 2005; Celik and Ma 2011), fuzzy c-means (Ghosh, Mishra, and Ghosh 2011), etc.

The emergence of very high resolution (VHR) remote sensing image and the rapid increase in computational capabilities over the last decade have challenged the traditional change detection methods (Hussain et al. 2013), such as geo-referencing accuracy, larger reflectance variability in each class and different acquisition characteristics, due to VHR images include a more valuable and abundant information. The large volume of information presented in VHR images often results in much more unnecessary change detections than other kinds of images, which is known as the "salt and pepper" effect. Furthermore, the potential accuracy of traditional change detection methods would be also reduced by such characteristics of VHR. In the last years, some novel approaches have been developed which take the relationship between spatially adjacent pixels into account. Spatial-context information can be modelled by fixed-shape neighborhood systems for the texture information extraction(Bruzzone and Bovolo 2013). Under the extraction, texture-information-based change detection method is proved to be useful in several studies (Smits and Annoni 2000; He et al. 2011; Klaric et al. 2013; Li and Leung 2002). Though texture information is commonly robust in its change detection performance, the existing texture difference measure is not completely suitable since most of the difference measures are pixel-wised and different texture features have the same weights. Therefore, the texture-based algorithm needs to be researched deeply and a more efficient texture difference measure should be presented.

To address the aforementioned problem, a novel unsupervised change detection approach is proposed by utilizing local-similarity-based texture difference measure (LSTDM) in this paper. In LSTDM, a local similarity between two temporal gray level co-occurrence matrix (GLCM) (Haralick, Shanmugam, and Dinstein 1973) texture images is defined to identify the changes. In addition, the coefficient of variation method (Liu 2015) is applied to define the weight among different GLCM texture features. In order to generate a more accurate resulting change map, the unsupervised change detection problem in VHR remote sensing images is formulated as minimizing an energy function related with changed and unchanged classes in the difference image. A modified expectation maximization based Chan-Vese active contour model (C-V) (Chan and Vese 2001) is applied to the difference image for separating the changed and unchanged regions. As shown in Fig. 1, the proposed approach is made up three blocks as follows. First, the GLCM texture features are extracted from multitemporal VHR remote sensing images, respectively. Then, the difference image was generated based on LSTDM. Finally, a modified expectation-maximization-based C-V model is applied to obtain the final change map.

Insert Fig.1 here.

2 Proposed change detection approach

Let $\mathbf{X}_1$ and $\mathbf{X}_2$ be two VHR remote sensing images acquired in same geographical area at times t_1 and t_2, which have been co-registered and radiometrically corrected and have the same size of $M \times N$.

2.1 Local similarity based texture difference measure

In previous research, a distance between two GLCM texture image pixels was applied as the difference measure (Smits and Annoni 2000) and it was proved to be robust for misregistration. However, the distance-based texture difference measure is a pixel-based method and ignores the spatial relationship of texture features. As shown in Fig. 2(a) and 2(b), two texture image chips were acquired at times t_1 and t_2 respectively. The target pixel is labelled by P. In the previous texture difference measure, the pixel P will be directly classified as unchanged pixels. However, the change detection result is not completely reasonable because the two temporal texture image chips are not coincident as can be seen in Fig. 2. In addition to the aforementioned problem, it is not completely reasonable that the different texture feature has the same weight.

Insert Fig. 2 here.

To address the two problems, LSTDM is proposed in this paper. First, a local similarity measure between two temporal GLCM texture image chips is defined. This measure translates the difference of the target pixel P at times t_1 and t_2 into the similarity of the pixels in its neighbours (as shown in the square frame of Fig. 2). The local similarity measure, which represented by $S_f\left(t_1,t_2\right)$, can be formulated as

$$S_f\left(t_1,t_2\right)=\frac{1}{1+d_f\left(t_1,t_2\right)} \tag{1}$$

where

$$d_f\left(t_1,t_2\right)=\sqrt{\left(\frac{1}{n}\sum_{(u,v)\in\omega}\left(f^{t_1}\left(u,v\right)-f^{t_2}\left(u,v\right)\right)^2\right)}. \tag{2}$$

In which, $d_f\left(t_1,t_2\right)$ denotes the Euclidean distance of the local texture feature at times t_1 and t_2, $f\left(u,v\right)$ is the feature value at the position $\left(u,v\right)$, and ω means the 3×3 neighborhood centered at P. n presents the number of pixels in the neighbours.
Then, in order to discriminate the contribution of different texture features, the coefficient of variation method is utilized. This method has already proved effectively in weight determination (Liu 2015). The weight of the feature f, which represented by W_f, can be calculated using the following equation,

$$W_f=\frac{V_f}{\sum_f^F V_f},V_f=\frac{\sigma_f}{\mu_f} \tag{3}$$

where V_f denotes the coefficient of variation of feature f, μ_f and σ_f are the mean value and the variance of feature f, respectively.
Finally, LSTDM, which represented by $D\left(t_1,t_2\right)$, can be formulated as

$$D\left(t_1,t_2\right)=\sum_f^F\frac{W_f}{S_f\left(t_1,t_2\right)} \tag{4}$$

where F is the total number of the GLCM features extracted in VHR images.

2.2 Expectation maximization based level set method

After obtaining the difference image X calculated by LSTDM, a change detector is acquired to generate the resulting change map. Considering texture information is regional, the threshold-based change detection methods are not completely suitable. In recent years, level set based method is successively proved to be an effective region-based change detection method (Bazi, Melgani, and Al-Sharari 2010; Hao et al. 2014). In this method, the selection of the initial contour is crucial to the result. To this end, an expectation maximization based C-V model (EMCVM), is introduced to generate the change map in this paper. In EMCVM, a suitable initial contour can be generated by EM and morphology operation. The details are described in the following sections.

2.2.1 Generation of the initial change map by EM

In this paper, it is assumed that the difference image X calculated by LSTDM can be seen as a Gaussian mixture density distribution consisting of two density components associated with changed and unchanged class, i.e.,

$$p(X) = p(X/W_1)P(W_1) + p(X/W_2)P(W_2) \tag{5}$$

Where $p(X)$, $p(X/W_1)$ and $p(X/W_2)$ are the probability density functions of the difference image X, changed pixels W_1 and unchanged pixels W_2, and $p(W_1)$ and $p(W_2)$ are the a priori probabilities of changed pixels and unchanged pixels, respectively. The probability density functions $p(X/W_k)$, where $k \in (1,2)$, can be calculated by Gaussian model.

Step1. Initialize the means μ_k, variance σ_k^2 and a priori probability $P(W_k)$. The initial value of the estimates can be determined by exploiting the intrinsic characteristics of the difference image obtained with the LSTDM. A k-means cluster algorithm was utilized to obtain the initial changed and unchanged pixels. The value of μ_k, σ_k^2 and $P(W_k)$ can then be computed from the classified pixels and regarded as the initial values to EM.

Step2. Expectation step. Equation (5) is used to evaluate the posterior probability $P(W_k/x_i)$ with (6), as follows:

$$P(W_k/x_i) = \frac{P(W_k)\,p(x_i/W_k)}{P(x_i)} \tag{6}$$

Here, $1 \le i \le MN$ and x_i is the ith pixel of the difference image.

Step 3. Maximization step. Re-estimate the parameters using the following equations.

$$P^{t+1}(W_k) = \frac{\sum_{i=1}^{MN} P^t(W_k/x_i)}{MN} \tag{7}$$

$$\mu_k^{t+1} = \frac{\sum_{i=1}^{MN} P^t\left(W_k / x_i\right) x_i}{\sum_{i=1}^{MN} P^t\left(W_k / x_i\right)} \tag{8}$$

$$\left(\sigma_k^2\right)^{t+1} = \frac{\sum_{i=1}^{MN} P^t\left(W_k / x_i\right)\left(x_i - \mu_k\right)^2}{\sum_{i=1}^{MN} P^t\left(W_k / x_i\right)} \tag{9}$$

where the superscripts t and t+1 are the current and next iterations, respectively. The parameters are estimated by the steps above, and then checked for convergence. If the convergence criterion is not satisfied, repeat steps 2 and 3 until convergence is achieved.

Step 4. Get the initial change map. On the basis of the estimates of the statistical terms obtained by the EM algorithm, the optimum threshold value can be estimated by solving the following equation with respect to the variable X. In the end, using the threshold method, the initial change map can be generated.

$$\frac{P\left(W_1\right)}{P\left(W_2\right)} = \frac{p\left(X / W_2\right)}{p\left(X / W_1\right)} \tag{10}$$

2.2.2 Morphology operation

Despite the effectiveness of the EM method, it is not completely reasonable that the EM method is developed under the assumption that pixel values are independent of one another. For this reason, there are still many errors presented inside and outside the change map. To improve the performance, two morphology operations are applied in this paper.

(1) Morphological opening operation: This operation is a filter based on geometric operation, which can remove isolated points. Using this operation, errors outside the changed class can be removed.

(2) Morphological closing operation: This operation is a filter by filling the image concave, which can be used to fill the hole in the image. Using this operation, those holes inside changed class can be filled. In this way, a much better initial contour is obtained.

2.2.3 Generation of the final change map by level set

The changed pixels in the difference image can be seen as the object and extracted by finding an optimal contour C by the energy functional $E\left(C\right)$ given as,

$$E\left(C\right) = \int_{I(C)} \left|x_i - c_1\right|^2 dxdy + \int_{O(C)} \left|x_i - c_2\right|^2 dxdy + \nu\left|C\right| \tag{11}$$

where C is the evolving contour, $I\left(C\right)$ represents the area inside the evolving contour and can be seen as changed pixels, $O\left(C\right)$ denotes the area outside the evolving contour and can be regarded as unchanged pixels, x_i denotes the ith pixel

value of the difference image, c_1 and c_2 denote the mean value of inside and outside the evolving contour respectively.

To solve the minimal partition problem, the level set method is utilized. In the level set method, Ω represents the image domain and the curve C is represented by the zero level set of Lipchitz function φ, such that

$$\begin{aligned}&(x,y)\in\Omega:\varphi(x,y)>0, if\ (x,y)\in I(C)\\&(x,y)\in\Omega:\varphi(x,y)=0, if\ (x,y)\in C\\&(x,y)\in\Omega:\varphi(x,y)<0, if\ (x,y)\in O(C).\end{aligned}\tag{12}$$

The energy function can be described using level set function φ instead of unknown variable C, and (11) can be written as

$$\begin{aligned}E(\varphi)=&\int_\Omega|x_i-c_1|^2H(\varphi)dxdy+\int_\Omega|x_i-c_2|^2(1-H(\varphi))dxdy\\&+\nu\int_\Omega\delta(\varphi)|\nabla\varphi|dxdy\end{aligned}\tag{13}$$

where $\nabla\varphi$ means the gradient of φ, $H(\varphi)$ denotes the Heaviside function and formulated as follows,

$$H_\varepsilon(z)=\frac{1}{2}\left(1+\frac{2}{\pi}\arctan\left(\frac{z}{\varepsilon}\right)\right),\delta_\varepsilon(z)=\frac{1}{\pi}\frac{\varepsilon}{\varepsilon^2+z^2}\tag{14}$$

On the basis of the above, the next steps are implemented iteratively until the optimal φ is obtained.

Step1. Initialize φ^n by the contour created by EM and morphology operation step, n=0.

Step2. Compute $c_1(\varphi^n)$ and $c_2(\varphi^n)$. Keep φ fixed, the energy functional is minimized with respect to c_1 and c_2, and they can be generated by

$$c_1=\frac{\int_\Omega x_iH(\varphi)dxdy}{\int_\Omega H(\varphi)dxdy}\tag{15}$$

$$c_2=\frac{\int_\Omega x_i(1-H(\varphi))dxdy}{\int_\Omega(1-H(\varphi))dxdy}\tag{16}$$

Step3. Solve the partial differential equation (PDE) in φ from (17), to obtain φ^{n+1}. Keep c_1 and c_2 fixed, the PDE with respect to φ is given as follows,

$$\frac{\partial\varphi}{\partial t}=\delta_\varepsilon(\varphi)\left[\nu\mathrm{div}(\nabla\varphi/|\nabla\varphi|)-(x_i-c_1)^2+(x_i-c_2)^2\right]\tag{17}$$

Check whether the solution is stationary. If not, n=n+1 and repeat step 2 and step 3.
In this way, the final result change map can be obtained.

3 Experiments and results

To evaluate the performance of the proposed change detection method, two temporal VHR remote sensing image data sets were tested. For quantitative evaluation, the change maps generated by the two data sets are respectively compared with the ground truth images, which were produced by manual digitization, using three evaluation indices.

(1) Miss detection N_m is the number of unchanged pixels in the change detection result, which were classified in the changed class in the ground truth image. The miss detection rate P_M can be formulated as $P_M=N_m/N_c$, where N_c is the total number of changed pixels counted in the ground truth image.

(2) False Alarm N_f is the number of changed pixels in the change detection result, which were classified in the unchanged class in the ground truth image. The false alarm rate P_F can be formulated as $P_F= N_f /N_u$, where N_u is the total number of unchanged pixels counted in the ground truth image.

(3) Total Error N_t is the number of incorrectly detected pixels, which include miss detection and false alarm. The total error rate P_T can be formulated as $P_T= (N_m+N_f)/(N_c+N_u)$.

In order to verify the effectiveness of the proposed method, it is compared with the state-of-the-art methods, such as fuzzy C-means (FCM) (Ghosh, Mishra, and Ghosh 2011), expectation maximization (EM) (Bruzzone and Prieto 2000), markov random field (MRF) (Bruzzone and Prieto 2000), C-V model (Chan and Vese 2001) and expectation maximization based level set (EMLS) (Hao et al. 2014), respectively. The parameter values used in the experiments are given as follows: the size of the window is 3×3 for GLCM, ω=3 for LSTDM, ν=0.1 and the step Δt=0.1 for level set.

3.1 Feature selection

Because it is not a truth that "the more features integrated, the better the performance", and different features' contribution for change detection are inconsistent. Feature selection is needed in LSTDM. In order to further explore the impacts of different features, we arranged and built different feature-fusion data sets, performed change detection using the proposed method to analyse and compare the experimental results. With the same training samples and same parameters, different feature sets were tested, and the corresponding overall accuracy as shown in Fig. 3.

Insert Fig. 3 here.

From the results in Fig. 3, some observations can be concluded: the mean texture feature have the most accurate performance among eight features; as the mean, homogeneity, entropy and second moment features are the first four texture features in change detection. Therefore, the four texture features were used in LSTDM to obtain the texture difference image.

3.2 Experiment 1

The first data set used in the experiments includes two VHR images of size 508×508 pixels acquired by Satellite Probatoire d'Observation de la Terre 5 (SPOT5) collected on the city of Tianjin province of China on April 2008 and February 2009, respectively, and they were generated by fusing panchromatic and multispectral images, which had three bands. The spatial resolution of this data set is 2.5 m. the ground truth of the change detection map shown in Fig. 4(c) was manually created based on the input images shown in Fig. 4(a) and Fig. 4(b).

Insert Fig. 4 here.

First, the GLCM features including mean, homogeneity, entropy and second moment were extracted, Then LSTDM was applied to obtain the texture difference image. To compare with LSTDM, the traditional difference image was generated by CVA using the spectral information from the first data set. The histograms of the two difference images are shown in Fig. 5. As can be seen from Fig. 5(a), the separation between the changed and unchanged classes is not very clear. This makes it difficult to partition the difference image into two such classes. On the other hand, one can observe two peaks in Fig. 5(b), and they are far apart from each other. This makes it much easier to separate the difference image into two classes for conducting the change detection.

Insert Fig. 5 here.

The modified C-V model was utilized to detect changes from the difference image of LSTDM at the basis of the generation of initial contour, which was obtained by EM method and morphology operation. The change map generated by proposed method was shown in Fig. 6(f). Fig. 6(a)-(e) show the change maps resulted from FCM, EM, MRF, C-V, EMLS, respectively.

Insert Fig. 6 here.

As shown in Fig. 6(a) and (b), EM and FCM method produce much "salt and pepper" noise without considering contextual information as presented in the A region of Fig. 6(a) and 6(b). MRF method decrease such influence while another problem, namely over-smooth, and was introduced simultaneously as shown in Fig.6 (c). C-V model not only yields more homogenous regions but preserves detailed change information while MRF produces over-smooth result as shown in the B region of Fig. 6(c) and 6(d). However, a suitable initial contour should to be prepared in C-V model. EMLS also have the advantage with C-V model, but it is sensitive with the changed and unchanged class centres. As shown in the C region of Fig. 6, the proposed method can preserve detailed change information and decrease over-smooth without pre-setting initial contour. The reason is that LSTDM includes more abundant detailed information and the modified C-V model can generate more accurate change map. Table 1 presents the accuracy comparisons of N_m, N_f and N_t among FCM, EM, MRF, C-V, EMLS and proposed method. It is found that the proposed method generates the most accurate result than other methods, because LSTDM include more detailed

information by integrate texture features and the modified region based C-V model can identify the changed and unchanged class accurately.

Insert table 1 here.

3.3 Experiment 2

The second data set contains two VHR images (778×544 pixels) of the city of Wuhan, China, which were acquired on April 1, 2002 (Fig. 7(a)) and July 16, 2009 (Fig. 7(b)) by the QuickBird satellite. The instrument's pixel resolution is 2.4 m. The ground truth map shown in Fig. 7(c) was manually created based on the input images.

Insert Fig. 7 here.

On the basis of the above, four texture features (mean, homogeneity, entropy and second moment) were generated by GLCM. Then LSTDM was applied to obtain the texture difference image. To demonstrate the LSTDM outstanding performance for change detection to other measures, the traditional difference image was generated by CVA using the spectral information of the data set. Histograms of the difference images resulted from two test images are shown in Fig. 8. As can be seen from Fig. 8(a), the grey value distribution of the CVA difference image is not balanced. Therefore, it is difficult to separate the changed and unchanged classes. On the contrary, the grey value distribution of LSTDM shown in Fig. 8(b) obeys a Mixed Gaussian distribution. This makes it much easier to separate the difference image into two classes for conducting the change detection.

Insert Fig. 8 here.

The EM method and morphological operation were applied to generate the initial contour for the next step. Then the modified C-V model was utilized to detect changes in the difference image generated by LSTDM. The change map generated by proposed method was shown in Fig. 9(f). Fig. 9(a)-(e) show the change maps resulted from FCM, EM, MRF, C-V, EMLS, respectively.

Insert Fig. 9 here.

Fig. 9(a)-(c) present the change maps of three pixel-based change detection methods, namely EM, FCM and MRF. The first two methods produce much "salt and pepper" noise (as shown in the A region of Fig.9) without considering contextual information, and the third method can get better result by utilizing neighbourhood information. As shown in the B region of Fig. 9(c)-(e), C-V model and EMLS preserve detailed change information by gather more homogenous regions and avoid over-smooth results at the same time. However, the selection of initial contour has an important effect on the performance of C-V model. The result generated by EMLS is sensitive to the changed and unchanged class centres. In this paper, the proposed method not only preserves detailed information, but decreases over-smooth phenomenon without

pre-setting initial contour (as shown in the C region of Fig.9). The reason is that more abundant texture information was generated by LSTDM and more accurate change map can be obtained by the modified C-V model. Table 2 presents the accuracy comparisons of false alarm, missed detection and total error between FCM, EM, MRF, C-V, EMLS and proposed method. It is found that the proposed method generates the most accurate result among methods used in this study, because LSTDM include more detailed information by integrate texture features and the modified region based C-V model can identify the changed and unchanged class accurately.

Insert table 2 here.

4 Conclusion

In this paper, an unsupervised change detection method based on GLCM texture features was proposed and applied to VHR remote sensing images. The proposed algorithm utilized LSTDM to obtain the difference image. The EMACM then used to generate the final change map. Experimental results showed that the proposed method can sufficiently increase the robustness with respect to noise and spectral similarity, and it can obtain the highest accuracy compared with EM, FCM, MRF, C-V model and EMLS.

Even through the proposed method can produce more accurate change detection result, there are still some works need to be deeply researched. In this paper, the GLCM texture information was applied only. Hence, other texture extraction methods should be utilized, and fusion based methods is worth to research.

Funding

The work presented in this paper is supported by the National Natural Science Foundation of China [41331175]; a Project Funded by the Priority Academic Program Development of Jiangsu Higher Education Institutions; the Fundamental Research Funds for the Central Universities under Grant 2015XKQY09; the Natural Science Foundation of Jiangsu Province [grant number BK20160248].

References

Bazi, Y., L. Bruzzone and F. Melgani. 2005. "An Unsupervised Approach Based on the Generalized Gaussian Model to Automatic Change Detection in Multitemporal Sar Images." *IEEE Transactions on Geoscience and Remote Sensing* 43:874-887.

Bazi, Y., F. Melgani and H. D. Al-Sharari. 2010. "Unsupervised Change Detection in Multispectral Remotely Sensed Imagery with Level Set Methods." *IEEE Transactions on Geoscience and Remote Sensing* 48:3178-3187.

Bovolo, F. and L. Bruzzone. 2005. "A Detail-Preserving Scale-Driven Approach to Change Detection in Multitemporal Sar Images." *IEEE Transactions on Geoscience and Remote Sensing* 43:2963-2972.

Bovolo, F., L. Bruzzone and M. Marconcini. 2008. "A Novel Approach to Unsupervised Change Detection Based on a Semisupervised Svm and a Similarity Measure." *IEEE Transactions on Geoscience and Remote Sensing* 46:2070-2082.

Bruzzone, L. and F. Bovolo. 2013. "A Novel Framework for the Design of Change-Detection Systems for Very-High-Resolution Remote Sensing Images." *Proceedings of the IEEE* 101:609-630. doi: 10.1109/jproc.2012.2197169.

Bruzzone, L. and D. F. Prieto. 2000. "Automatic Analysis of the Difference Image for Unsupervised Change Detection." *IEEE Transactions on Geoscience and Remote Sensing* 38:1171-1182.

Celik, T. and K.-K. Ma. 2011. "Multitemporal Image Change Detection Using Undecimated Discrete Wavelet Transform and Active Contours." *IEEE Transactions on Geoscience and Remote Sensing* 49:706-716.

Chan, T. F. and L. A. Vese. 2001. "Active Contours without Edges." *IEEE Transactions on Image processing* 10:266-277.

Ghosh, A., N. S. Mishra and S. Ghosh. 2011. "Fuzzy Clustering Algorithms for Unsupervised Change Detection in Remote Sensing Images." *Information Sciences* 181:699-715.

Hao, M., W. Shi, H. Zhang and C. Li. 2014. "Unsupervised Change Detection with Expectation-Maximization-Based Level Set." *IEEE Geoscience and Remote Sensing Letters* 11:210-214. doi: 10.1109/lgrs.2013.2252879.

Haralick, R. M., K. Shanmugam and I. H. Dinstein. 1973. "Textural Features for Image Classification." *IEEE Transactions on Systems, Man and Cybernetics*:610-621.

He, C., A. Wei, P. Shi, Q. Zhang and Y. Zhao. 2011. "Detecting Land-Use/Land-Cover Change in Rural–Urban Fringe Areas Using Extended Change-Vector Analysis." *International Journal of Applied Earth Observation and Geoinformation* 13:572-585.

He, P., W. Shi, H. Zhang and M. Hao. 2014. "A Novel Dynamic Threshold Method for Unsupervised Change Detection from Remotely Sensed Images." *Remote Sensing Letters* 5:396-403. doi: 10.1080/2150704x.2014.912766.

Hussain, M., D. Chen, A. Cheng, H. Wei and D. Stanley. 2013. "Change Detection from Remotely Sensed Images: From Pixel-Based to Object-Based Approaches." *ISPRS Journal of Photogrammetry and Remote Sensing* 80:91-106.

Klaric, M. N., B. C. Claywell, G. J. Scott, N. J. Hudson, O. Sjahputera, Y. Li, S. T. Barratt, J. M. Keller and C. H. Davis. 2013. "Geocdx: An Automated Change Detection and Exploitation System for High-Resolution Satellite Imagery." *IEEE Transactions on Geoscience and Remote Sensing* 51:2067-2086.

Li, L. and M. K. Leung. 2002. "Integrating Intensity and Texture Differences for Robust Change Detection." *IEEE Transactions on Image Processing* 11:105-112.

Liu, S. T. 2015. "A Mathematical Programming Approach to Sample Coefficient of Variation with Interval-Valued Observations." *TOP*:1-18.

Lu, D., P. Mausel, E. Brondizio and E. Moran. 2004. "Change Detection Techniques." *International Journal of Remote Sensing* 25:2365-2401.

Prieto, L. B. and D. Fernandez. 2000. "A Minimum-Cost Thresholding Technique for Unsupervised Change Detection." *International Journal of Remote Sensing* 21:3539-3544.

Smits, P. C. and A. Annoni. 2000. "Toward Specification-Driven Change Detection." *IEEE Transactions on Geoscience and Remote Sensing* 38:1484-1488.

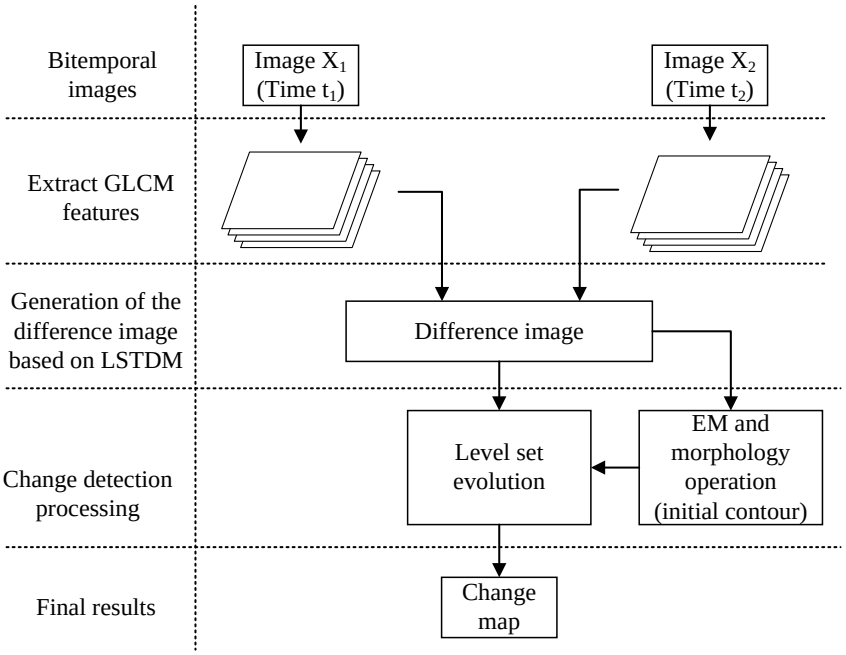

Fig. 1. General scheme of the proposed approach.

Fig. 2. Two temporal texture image chips.

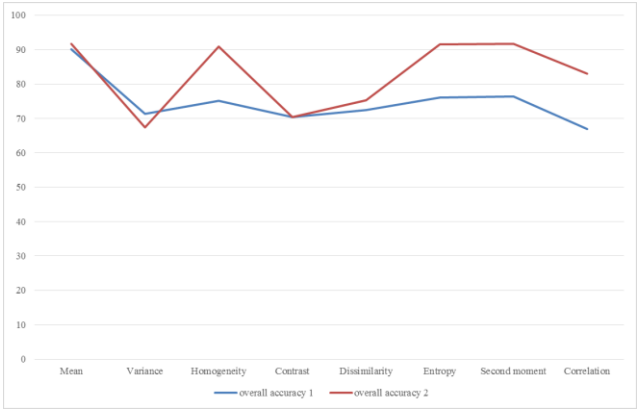

Fig. 3. The line chart of total accuracy of different texture features.

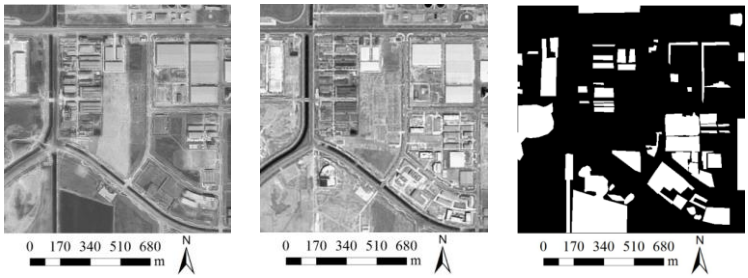

(a) (b) (c)

Fig. 4. SPOT5 data set used in experiment 1.

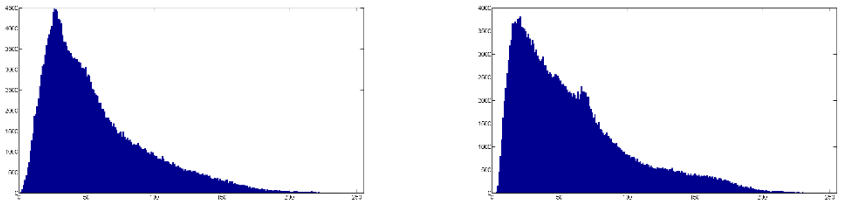

(a) (b)

Fig. 5. Histograms of the difference images which resulted from two test images of experiment 1. (a) Difference image generated by CVA. (b) Difference image generated by LSTDM.

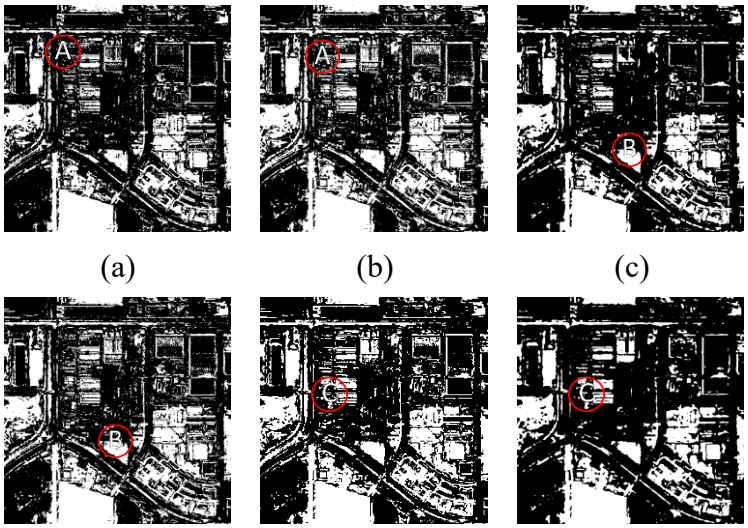

(a) (b) (c)

(d) (e) (f)

Fig. 6. Change detection results of data set 1 obtained by (a) FCM, (b) EM, (c) MRF, (d) C-V, (e) EMLS, (f) proposed.

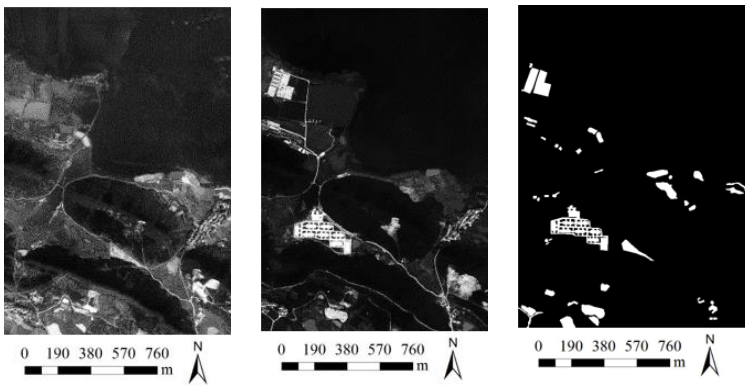

(a) (b) (c)

Fig. 7. QuickBird data set used in experiment 2.

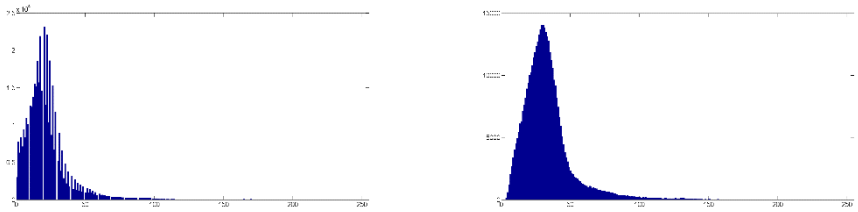

(a) (b)

Fig. 8. Histograms of the difference images which resulted from two test images of experiment 2. (a) Difference image generated by CVA. (b) Difference image generated by LSTDM.

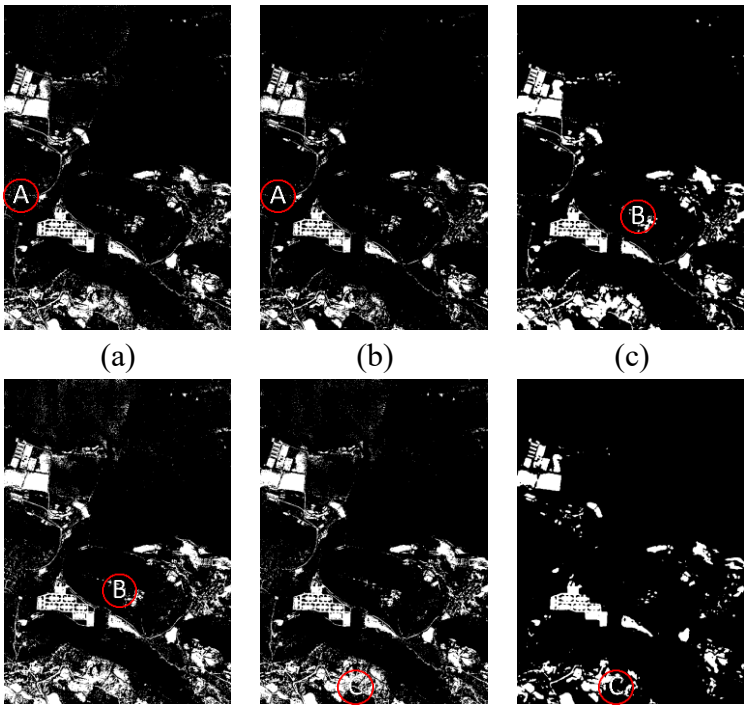

(a) (b) (c)

(d) (e) (f)

Fig. 9. Change detection results of data set 2 obtained by (a) FCM, (b) EM, (c) MRF, (d) C-V, (e) EMLS, (f) proposed.

Table 1. Quantitative change detection results for the data set 1.

Method	False Alarms		Miss Detections		Total Errors	
	pixels	P_F (%)	pixels	P_M (%)	pixels	P_T (%)
FCM	37907	19.21	11745	19.35	49652	19.24
EM	39732	20.13	11345	18.69	51077	19.79
MRF	28096	14.24	14788	24.36	42884	16.62
C-V	25541	12.94	12761	21.02	38302	14.84
EMLS	36444	18.47	10558	17.39	47002	18.21
Proposed	20784	10.53	11392	18.76	32176	12.47

Table 2. Quantitative change detection results for the data set 2.

Method	False Alarms		Miss Detections		Total Errors	
	pixels	P_F (%)	pixels	P_M (%)	pixels	P_T (%)
FCM	41463	10.22	3559	20.27	45022	10.64
EM	30576	7.54	4054	23.09	34630	8.18
MRF	22210	5.47	4771	27.17	26981	6.37
C-V	31276	7.71	3394	19.33	34670	8.19
EMLS	30302	7.47	4091	23.30	34393	8.13
Proposed	16963	4.18	4421	25.18	21384	5.05